Catalysis Science & Technology

PAPER

View Article Online
View Journal | View Issue

Cite this: *Catal. Sci. Technol.*, 2016, 6, 4511

An oxygen pool from $YBaCo_4O_7$-based oxides for soot combustion†

Guangkai Tian,[a] Hui Chen,[a] Chenxi Lu,[a] Ying Xin,[a] Qian Li,[a] James A. Anderson[b] and Zhaoliang Zhang*[a]

Received 15th December 2015,
Accepted 5th February 2016

DOI: 10.1039/c5cy02181b

www.rsc.org/catalysis

Soot, often referred to as black carbon emitted from diesel engines, is not only a particulate matter pollutant but also a light-absorbing agent that may affect global climate, but can be effectively controlled using a catalytic diesel particulate filter (DPF). A new $YBaCo_4O_{7+\delta}$-type oxygen storage material is reported as an effective catalyst for soot combustion. Isotopic isothermal reactions demonstrate the activation of gaseous oxygen and subsequent oxygen storage and reaction/desorption during an oxidation process. High activity and structural stability are achieved by the substitution of Co with Al and Ga to form $YBa(Co_{0.85}Al_{0.075}Ga_{0.075})_4O_{7+\delta}$. The specific rates at 300 °C of $YBaCo_4O_{7+\delta}$ and $YBa(Co_{0.85}Al_{0.075}Ga_{0.075})_4O_{7+\delta}$, normalized by surface areas, are an order of magnitude higher than those of CeO_2-based oxides. This kind of oxygen-storage material acts as an oxygen pool, which ensures that the accumulated soot on a DPF can be promptly combusted.

1. Introduction

Soot, often referred to as black carbon, is not only a particulate matter pollutant but also a light-absorbing agent that may affect global climate.[1] Diesel engines are amongst the most abundant emission sources of soot that can be effectively controlled by a catalytic diesel particulate filter (DPF).[2] Commercial catalysts are composed of noble metals (Pt and Pd) supported on ceria-based oxides,[3] oxidizing NO into NO_2, which is transported through a gas phase to soot aggregates where it oxidizes carbon while being reduced to NO.[4] A so-called continuously regenerated trap (CRT) overcomes the problem of poor contact between soot and a catalyst. However, the limited amounts of NO_x present and the need to control NO_x for Euro IV standards are not ideal situations to meet the requirements of the latest generation of diesel engines, leading to a drive to develop catalysts which can produce highly reactive oxygen species from gaseous O_2 molecules.[5,6]

Among this kind of catalysts, the extensively studied soot oxidation catalysts are ceria-based oxides due to the redox properties of the Ce^{3+}/Ce^{4+} couple and the capacity of ceria to exchange oxygen with a gas phase.[7–12] Unfortunately, the effective utilization of such active oxygen species is limited by the extent of contact between soot and a catalyst. This limitation could be overcome by producing a sufficiently high amount of active oxygen to ensure that, at least, a proportion reaches the soot particle surface.[5]

In comparison with a conventional oxygen storage material, CeO_2–ZrO_2, $YBaCo_4O_7$ (114 structure) shows a markedly larger oxygen storage capacity (OSC), particularly at low temperatures (200–400 °C), which is just within the range of temperatures reached at the exhaust of a diesel engine.[13–16] The extraordinary oxygen storage capability of the $YBaCo_4O_7$-based oxides is due to the variable valence of Co ions between Co^{2+} and Co^{3+}. The limitation of $YBaCo_4O_{7+\delta}$ is that it decomposes just above 600 °C in an oxygen-containing atmosphere, which limits its applications in catalytic combustion at elevated temperatures.[13] Recently, Karppinen and colleagues identified that an $YBa(Co_{0.85}Al_{0.075}Ga_{0.075})_4O_{7+\delta}$ phase, where Co is co-substituted by Al and Ga is stable up to high temperatures under oxidizing conditions,[16] which creates the potential for $YBa(Co_{0.85}Al_{0.075}Ga_{0.075})_4O_{7+\delta}$ to become a more effective catalyst for catalytic combustion.

In this paper, $YBaCo_4O_{7+\delta}$ and $YBa(Co_{0.85}Al_{0.075}Ga_{0.075})_4O_{7+\delta}$ were studied from the perspective of catalysis for diesel soot combustion. Their oxygen storage performance allows them to create an oxygen pool supply of active oxygen which is created from a gaseous phase.[17] Although $YBaCo_4O_{7+\delta}$ has been reported as a robust catalyst for H_2O_2 oxidation of cyclohexene in the liquid phase,[18] the present result is the first report on high-temperature oxidation reactions for this kind of non-stoichiometric transition metal oxide materials.

[a] *School of Chemistry and Chemical Engineering, Shandong Provincial Key Laboratory of Fluorine Chemistry and Chemical Materials, University of Jinan, No. 336, West Road of Nan Xinzhuang, Jinan 250022, PR China. E-mail: chm_zhangzl@ujn.edu.cn; Fax: +86 531 89736032; Tel: +86 531 89736032*
[b] *Surface Chemistry and Catalysis Group, Department of Chemistry, University of Aberdeen, Aberdeen AB24 3UE, UK*

† Electronic supplementary information (ESI) available: Textural properties and XRD patterns of the samples. See DOI: 10.1039/c5cy02181b

2. Experimental section

The $YBaCo_4O_7$-type samples were synthesized from a precursor powder prepared by an EDTA (ethylenediaminetetraacetic acid) and CA (citric acid) complex gel method,[13] using $Y(NO_3)_3{\cdot}6H_2O$, $Ba(NO_3)_2$, $Co(NO_3)_3{\cdot}6H_2O$, $Ga(NO_3)_3{\cdot}6H_2O$ and $Al(NO_3)_3{\cdot}9H_2O$ as the starting materials. The precursor powder was calcined in a muffle at 350 °C for 2 h, then pelletized and sintered in air at 1000 °C for 24 h, followed by rapid cooling to room temperature. Further thermal treatment at 300 °C under a pure O_2 flow for 2 h obtained $YBaCo_4O_{7+\delta}$ and $YBa(Co_{0.85}Al_{0.075}Ga_{0.075})_4O_{7+\delta}$.

X-ray powder diffraction (XRD) patterns were recorded on a Rigaku D/max-RC diffractometer employing Cu Kα radiation. Surface areas and pore size distributions were determined by N_2 adsorption–desorption at 77 K using a Micromeritics ASAP 2020 instrument after outgassing at 300 °C for 5 h prior to analysis.

Temperature programmed desorption of O_2 (O_2–TPD) experiments were conducted in a fixed-bed flow reactor. A 150 mg sample was heated under a flow of high purity O_2 (30 ml min^{-1}) at 300 °C for 1 h. After cooling to room temperature, high purity He was introduced. Desorption was started at a heating rate of 2 °C min^{-1} in He (30 ml min^{-1}). The desorbed O_2 was monitored by a quadruple mass spectrometer (MS, OminiStar 200, Balzers).

Temperature programmed reduction with H_2 (H_2–TPR) experiments were performed in a quartz reactor with a thermal conductivity detector (TCD) to monitor H_2 consumption. A 50 mg sample was pretreated *in situ* at 300 °C for 1 h under a flow of O_2 and cooled to room temperature in the presence of O_2. After purging with N_2, TPR was conducted at 10 °C min^{-1} up to 700 °C under a 30 mL min^{-1} flow of 5 vol% H_2 in N_2. To quantify the total amount of H_2 consumption, CuO was used as a calibration reference.

"Dynamic" OSC (DOSC) measurements with CO–O_2 pulses were carried out at 200–500 °C. CO (4% CO/1% Ar/He at 300 mL min^{-1} for 10 s) and O_2 (2% O_2/1% Ar/He at 300 mL min^{-1} for 10 s) streams were pulsed alternately with at a frequency of 0.05 Hz. A DOSC value was obtained by integrating the CO_2 formed during one CO–O_2 cycle and was expressed as μmol of O per gram of catalyst (μmol [O] g^{-1}). The concentration of CO_2 was determined using a MS.

Temperature programmed oxidation (TPO) reactions were conducted in a fixed bed micro reactor consisting of a quartz tube (6 mm i. d.). Printex-U from Degussa was used as the model soot. The soot was mixed with the catalyst in a weight ratio of 1 : 9 in an agate mortar for 30 min, which resulted in a tight contact between the soot and the catalyst. A 50 mg sample of the soot/catalyst mixture was pre-treated under a flow of He (50 mL min^{-1}) at 200 °C for 30 min to remove adsorbed species. After cooling to room temperature, a gas flow with 5 vol% oxygen in He was introduced and then TPO was initiated at a heating rate of 5 °C min^{-1} until 880 °C. For pure soot combustion (non-catalytic), the catalyst was substituted by silica. CO and CO_2 concentrations in the effluent gas were monitored using an online gas chromatograph (GC) (SP-6890, Shandong Lunan Ruihong Chemical Instrument Corporation, China) fitted with a methanator. The ignition temperature for soot combustion was evaluated by the value of T_{10}, which is defined as the temperature at which 10% of the soot is converted. The selectivity to CO_2 is defined as the percentage CO_2 outlet concentration divided by the sum of the CO_2 and CO outlet concentrations.

Isothermal reactions at 300 °C, at which a stable and low soot conversion (<15%) was achieved, were conducted within the kinetic regime. The reaction rate for soot combustion was obtained from the slope of the conversion lines with time. Specific rates normalized by BET surface areas and turnover frequency (TOF)[19] were used to characterize the activity for soot combustion.

An isotopic isothermal reaction was performed by switching the flowing gas from 1% $^{16}O_2$ to 1% $^{18}O_2$ diluted in Ar at 350 °C. 50 mg of a mixture of the soot and catalyst in a tight contact mode was employed. The effluent gas from the reactor was continuously monitored by a MS for all of the isotopic molecules of CO_2 (at m/z = 44, 46 and 48).

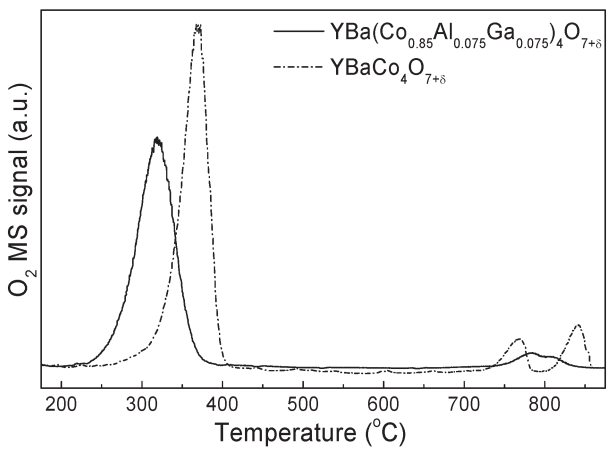

Fig. 1 O_2–TPD spectra of $YBaCo_4O_{7+\delta}$ and $YBa(Co_{0.85}Al_{0.075}Ga_{0.075})_4O_{7+\delta}$ from room temperature to 900 °C.

3. Results and discussion

The fresh $YBaCo_4O_{7+\delta}$ and $YBa(Co_{0.85}Al_{0.075}Ga_{0.075})_4O_{7+\delta}$ were confirmed to be composed of a single phase (Fig. S1†), similar to that of hexagonal $LuBaAlZn_3O_7$ (JCPDS 40-4099).[13] As the shifts in the XRD peaks for the separate substitution of Co by Al (r = 0.039 nm) and Ga (r = 0.047 nm) are opposed for each sample (Fig. S2†), the simultaneous substitution has a slight effect on the cell volume parameters. Furthermore, both ionic radii of Al and Ga are smaller than the high spin Co^{2+} ionic radius (r = 0.058 nm), thus Maignan *et al.* suggested that Al and Ga are substituted for Co^{3+}.[20] The BET surface areas are fairly low, in accordance with the high-temperature sintering preparation (Table S1†) and the highly crystalline nature of the samples.

In agreement with conclusions in the literature,[13,16] the O_2–TPD profiles (Fig. 1) show that both $YBaCo_4O_{7+\delta}$ and $YBa(Co_{0.85}Al_{0.075}Ga_{0.075})_4O_{7+\delta}$ desorb a large amount of oxygen below 400 °C, corresponding to δ = 0.37 and δ = 0.34, respectively. The peak maximum of $YBa(Co_{0.85}Al_{0.075}Ga_{0.075})_4O_{7+\delta}$ is 50 °C lower than that of $YBaCo_4O_{7+\delta}$, which suggests a promotion effect on O_2 desorption by doping, albeit with a slight decrease of the overall oxygen storage capability.[16] Above 700 °C, further desorption of O_2 is observed, corresponding to the possible decomposition of the 114 structure.[13] However, $YBa(Co_{0.85}Al_{0.075}Ga_{0.075})_4O_{7+\delta}$ shows less pronounced O_2 desorption than $YBaCo_4O_{7+\delta}$. After O_2–TPD at about 900 °C, the Y_2O_3 and CoO phases are segregated from $YBaCo_4O_{7+\delta}$, which is opposite to the stable structure of $YBa(Co_{0.85}Al_{0.075}Ga_{0.075})_4O_{7+\delta}$ (Fig. S3†).

A similar situation is observed in H_2–TPR (Fig. S1†). The 114 structure of $YBaCo_4O_{7+\delta}$ is completely destroyed by H_2 in TPR to 700 °C (Fig. S1a and b†). In contrast, $YBa(Co_{0.85}Al_{0.075}Ga_{0.075})_4O_{7+\delta}$ was preserved with no formation of new oxide phases (Fig. S1c and d†). The structural stability of $YBa(Co_{0.85}Al_{0.075}Ga_{0.075})_4O_{7+\delta}$ is vital to high-temperature redox reactions. As shown in Fig. 2, two peaks were observed for both $YBaCo_4O_{7+\delta}$ and $YBa(Co_{0.85}Al_{0.075}Ga_{0.075})_4O_{7+\delta}$. The low-temperature TPR peak can be assigned to the removal of non-stoichiometric excess O accommodated within the lattice, and the values of which are slightly larger than those consumed by δ (Table 1). The 114 structure of $YBaCo_4O_{7+\delta}$ is stable at this stage (Fig. S1a and b†). The second peak corresponds to the reduction of bulk and surface Co^{3+} of $YBaCo_4O_{7+\delta}$ and $YBa(Co_{0.85}Al_{0.075}Ga_{0.075})_4O_{7+\delta}$, respectively. The substitution of Co^{3+} by Al and Ga protects the structure from decomposition under reducing atmospheres (H_2–TPR and O_2–TPD).[20] Furthermore, the lower TPR temperature of $YBa(Co_{0.85}Al_{0.075}Ga_{0.075})_4O_{7+\delta}$ in comparison with that of $YBaCo_4O_{7+\delta}$ coincides with the O_2–TPD results.

Although H_2–TPR and O_2–TPD data may be useful in rapidly evaluating the potential OSC of the candidate materials, DOSC provides better simulation of instantaneous oscillations between lean (oxidizing) and rich (reducing) exhaust conditions during real operation and is therefore much more useful in the evaluation of the activity of OSC materials.[21] Fig. 3(a) shows the collected DOSC data and the corresponding transition curves at 320 °C of $YBa(Co_{0.85}Al_{0.075}Ga_{0.075})_4O_{7+\delta}$ as an example, with alternate dynamic pulses of 4% CO/1% Ar/He (10 s) and 2% O_2/1% Ar/He (10 s) under 0.05 Hz given in Fig. 3(b). In comparison with CeO_2–ZrO_2, the normalized DOSC values by the BET surface areas of $YBaCo_4O_{7+\delta}$ and $YBa(Co_{0.85}Al_{0.075}Ga_{0.075})_4O_{7+\delta}$ are more than thirty times larger (DOSC values of $YBaCo_4O_{7+\delta}$, $YBa(Co_{0.85}Al_{0.075}Ga_{0.075})_4O_{7+\delta}$ and $Ce_{0.43}Zr_{0.57}O_2$ at 400 °C are 40.9, 41.6 and 1.3 μmol [O] m^{-2}, respectively),[22] confirming the fast responses between reduction and oxidation environments. Furthermore, the higher DOSC of $YBa(Co_{0.85}Al_{0.075}Ga_{0.075})_4O_{7+\delta}$ in comparison with that of $YBaCo_4O_{7+\delta}$ is consistent with the O_2–TPD and H_2–TPR results.

The catalytic activity for soot combustion was first checked by TPO (Fig. 4a). $YBaCo_4O_{7+\delta}$ and $YBa(Co_{0.85}Al_{0.075}Ga_{0.075})_4O_{7+\delta}$ decrease from a T_{10} value of 530 °C for non-catalytic combustion to 387 and 379 °C, respectively, confirming the catalytic effect of the $YBaCo_4O_{7+\delta}$-type material and the higher activity of the latter than the former. In terms of the selectivity towards CO_2 formation, the non-catalytic combustion is only 43.3%, while $YBaCo_4O_{7+\delta}$ and $YBa(Co_{0.85}Al_{0.075}Ga_{0.075})_4O_{7+\delta}$ yield nearly 100% CO_2. After the TPO reactions, no phase decomposition occurs even for $YBaCo_4O_{7+\delta}$ (Fig. S4†), probably due to the high heating rate in 5 vol% oxygen in He.[23] Furthermore, the XRD peaks of $YBaCo_4O_{7+\delta}$ and $YBa(Co_{0.85}Al_{0.075}Ga_{0.075})_4O_{7+\delta}$ after TPO shift to higher angles, suggesting a lattice shrinkage, which confirms the participation of bulk oxygen.

The intrinsic activity was further demonstrated by kinetic rates at 300 °C, which can be obtained from the slope of the lines shown in Fig. 4b. As observed in Table 1, the specific rates of $YBaCo_4O_{7+\delta}$ and $YBa(Co_{0.85}Al_{0.075}Ga_{0.075})_4O_{7+\delta}$, normalized by BET surface areas, are an order of magnitude larger than that of $Ce_{0.43}Zr_{0.57}O_2$.[19–22] This is significant because 300 °C is a relevant temperature for light diesel engines. This particularly high reaction rate can ensure that the accumulated soot on the DPF can be readily combusted, leading to a lower balance point temperature (BPT) at which the rate of soot oxidation is matched with the rate of soot accumulation.[24] Furthermore, both the specific rate and TOF (Table 1) of $YBa(Co_{0.85}Al_{0.075}Ga_{0.075})_4O_{7+\delta}$ are a little higher than that of

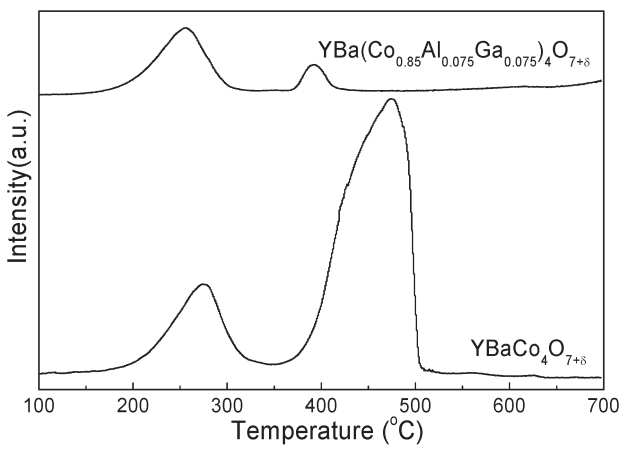

Fig. 2 H_2–TPR spectra of $YBaCo_4O_{7+\delta}$ and $YBa(Co_{0.85}Al_{0.075}Ga_{0.075})_4O_{7+\delta}$ from room temperature to 700 °C.

Table 1 H_2–TPR peak temperatures (T, °C), H_2 consumption (C, μmol g^{-1}), specific rates at 300 °C normalized by BET surface areas (mol s^{-1} $m^{-2} \times 10^{-8}$), and TOF ($s^{-1} \times 10^{-3}$) at 290 °C

Sample	Peak 1		Peak 2		Specific rates[a]	TOF
	T	C	T	C		
$YBaCo_4O_{7+\delta}$	275	74.9	475	298.5	2.11	1.34
$YBa(Co_{0.85}Al_{0.075}Ga_{0.075})_4O_{7+\delta}$	255	57.8	390	10.0	2.17	1.57

[a] The specific rate at 300 °C normalized by BET surface areas (80.4 m^2 g^{-1}) for $Ce_{0.43}Zr_{0.57}O_2$ is 0.21 mol s^{-1} $m^{-2} \times 10^{-8}$.

$YBaCo_4O_{7+\delta}$, confirming the higher intrinsic activity of $YBa(Co_{0.85}Al_{0.075}Ga_{0.075})_4O_{7+\delta}$.

In order to explore the origin of the active oxygen, isotopic isothermal oxidation at 350 °C was performed (Fig. 5). Before switching from $^{16}O_2$ to $^{18}O_2$ (to the left of the dashed line), the main product was $C^{16}O_2$, confirming that the soot oxidation occurs with the bulk oxygen species. The concentration of $C^{16}O_2$ for $YBa(Co_{0.85}Al_{0.075}Ga_{0.075})_4O_{7+\delta}$ is much larger than that for $YBaCo_4O_{7+\delta}$, which is again consistent with the O_2–TPD, H_2–TPR, DOSC, T_{10} and specific rates. After switching from $^{16}O_2$ to $^{18}O_2$ (to the right of the dashed line), the sum of the products of $C^{16}O^{18}O$, $C^{18}O_2$ and $^{16}O^{18}O$ still possesses higher concentrations of $YBa(Co_{0.85}Al_{0.075}Ga_{0.075})_4O_{7+\delta}$ than that of $YBaCo_4O_{7+\delta}$. However, the concentration of $C^{16}O_2$ decreased gradually to a very low value due to the depletion of $^{16}O_2$ in the gaseous phase. Comparatively, for both $YBaCo_4O_{7+\delta}$ and $YBa(Co_{0.85}Al_{0.075}Ga_{0.075})_4O_{7+\delta}$, the production of $C^{16}O^{18}O$ increases and then reaches a maximum, while the $C^{18}O_2$ production monotonically increases. This indicates that only the gaseous oxygen which has been activated by $YBaCo_4O_{7+\delta}$ and $YBa(Co_{0.85}Al_{0.075}Ga_{0.075})_4O_{7+\delta}$ can be used to oxidize the soot. In addition, the desorption of $^{16}O^{18}O$ is detected, which suggests that the desorbed $^{16}O^{18}O$ species do not interact with the soot to produce the product containing carbon, demonstrating that the intimate contact between the soot and catalysts is essential. Since the high DOSC can make up for the missing oxygen, the intrinsic activity of $YBaCo_4O_7$-based oxides is much more active than that of CeO_2-based oxides.

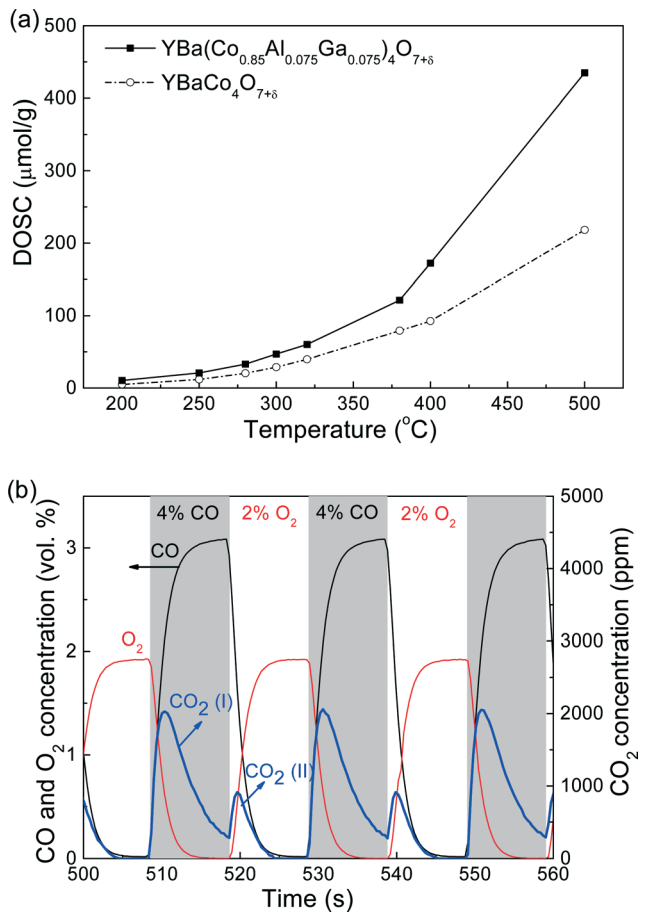

Fig. 3 DOSC of $YBaCo_4O_{7+\delta}$ and $YBa(Co_{0.85}Al_{0.075}Ga_{0.075})_4O_{7+\delta}$ (a) and enlarged transition curves of $YBa(Co_{0.85}Al_{0.075}Ga_{0.075})_4O_{7+\delta}$ (b) at 320 °C with dynamic pulses of 4% CO/1% Ar/He and 2% O_2/1% Ar/He under 0.05 Hz. CO_2(I) was produced by CO and surface oxygen; CO_2(II) was attributed to the reaction of absorbed CO and oxygen gas.[22]

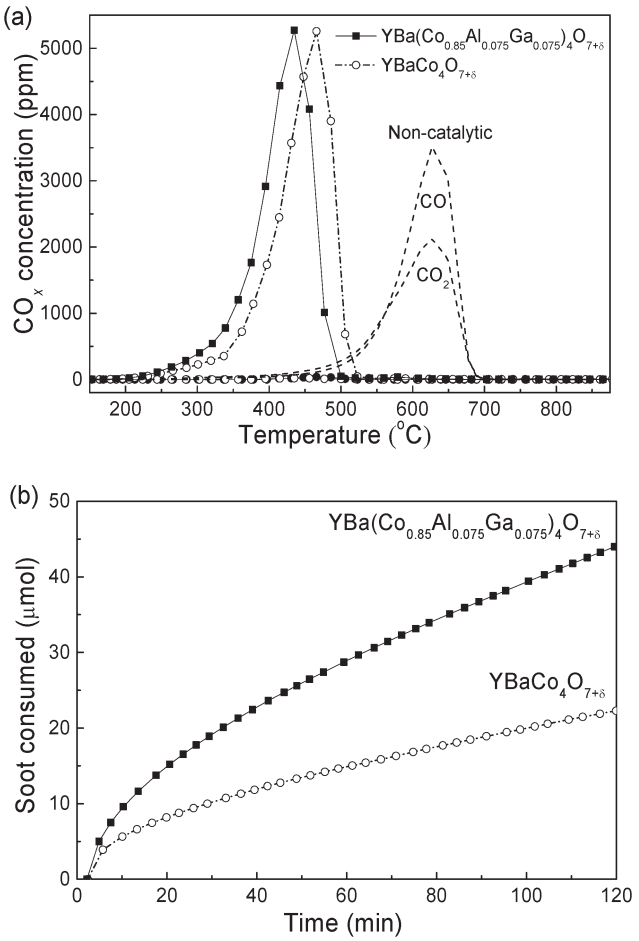

Fig. 4 TPO patterns of CO_x for soot combustion with O_2 over $YBaCo_4O_{7+\delta}$ and $YBa(Co_{0.85}Al_{0.075}Ga_{0.075})_4O_{7+\delta}$ (a); isothermal reactions for soot combustion at 300 °C within the kinetic regime (b) under tight contact conditions between the soot and catalysts.

Conclusions

In conclusion, a new $YBaCo_4O_{7+\delta}$-type oxygen storage material was used to catalyze soot combustion. Isotopic isothermal reactions demonstrate the activation of gaseous oxygen and subsequent oxygen storage and reaction/desorption during the oxidation process. Higher activity and structural stability are achieved by the substitution of Co with Al and Ga to form $YBa(Co_{0.85}Al_{0.075}Ga_{0.075})_4O_{7+\delta}$. The specific rates at 300 °C of $YBaCo_4O_{7+\delta}$ and $YBa(Co_{0.85}Al_{0.075}Ga_{0.075})_4O_{7+\delta}$, normalized by BET surface areas, are an order of magnitude larger than that of CeO_2-based oxides. This type of oxygen-storage material

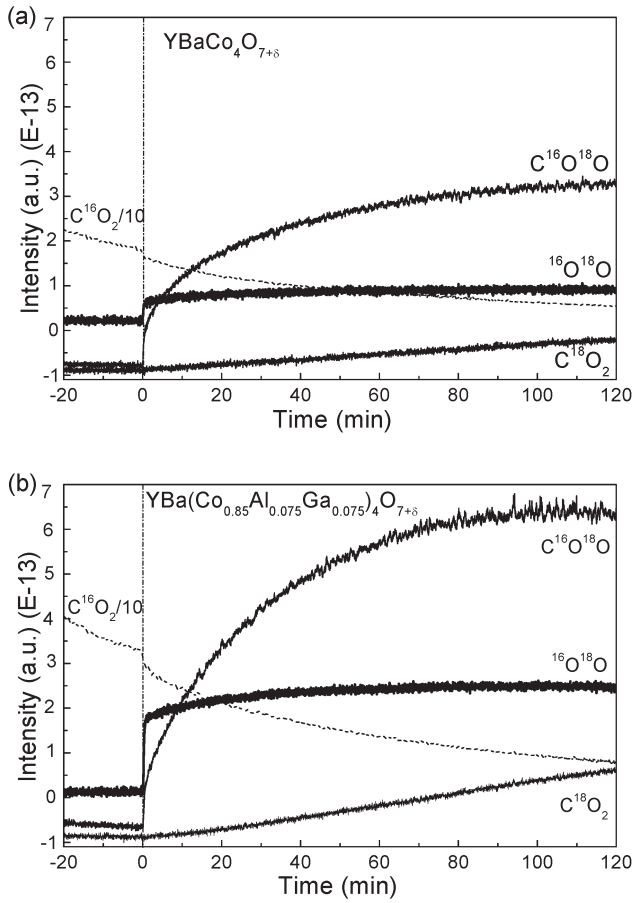

Fig. 5 Isothermal reactions for soot combustion at 350 °C after 1% $^{16}O_2$ was switched to 1% $^{18}O_2$ in He on $YBaCo_4O_{7+\delta}$ (a) and $YBa(Co_{0.85}Al_{0.075}Ga_{0.075})_4O_{7+\delta}$ (b).

provides an oxygen pool, which ensures that the accumulated soot on a DPF can be readily combusted.

Acknowledgements

This work is financially supported by the National Natural Science Foundation of China (no. 21477046, 21277060 and 21547007).

Notes and references

1 B. Booth and N. Bellouin, *Nature*, 2015, **509**, 167–168.
2 Barry A. A. L. van Setten, M. Makkee and J. A. Moulijn, *Catal. Rev.: Sci. Eng.*, 2001, **43**, 489–564.
3 S. Sumiya, L. Wang and G. Zhang, *SAE [Tech. Pap.]*, 2012, 2012-28-0009.
4 K. Leistner, A. Nicolle and P. Da Costa, *J. Phys. Chem. C*, 2012, **116**, 4642–4654.
5 I. Atribak, F. E. López-Suárez, A. Bueno-López and A. García-García, *Catal. Today*, 2011, **176**, 404–408.
6 E. Obeid, L. Lizarraga, M. N. Tsampas, A. Cordier, A. Boréave, M. C. Steil, G. Blanchard, K. Pajot and P. Vernoux, *J. Catal.*, 2014, **309**, 87–96.
7 Q. Liang, X. Wu, D. Weng and H. Xu, *Catal. Today*, 2008, **139**, 113–118.
8 J. Liu, Z. Zhao, J. Wang, C. Xu, A. Duan, G. Jiang and Q. Yang, *Appl. Catal., B*, 2008, **84**, 185–195.
9 E. Aneggi, C. de Leitenburg and A. Trovarelli, *Catal. Today*, 2012, **181**, 108–115.
10 A. Buenolopez, K. Krishna, M. Makkee and J. Moulijn, *J. Catal.*, 2005, **230**, 237–248.
11 K. Harada, T. Oishi, S. Hamamoto and T. Ishihara, *J. Phys. Chem. C*, 2014, **118**, 559–568.
12 A. Bueno-López, *Appl. Catal., B*, 2014, **146**, 1–11.
13 M. Karppinen, H. Yamauchi, S. Otani, T. Fujita, T. Motohashi, Y. H. Huang, M. Valkeapää and H. Fjellvåg, *Chem. Mater.*, 2006, **18**, 490–494.
14 S. Kadota, M. Karppinen, T. Motohashi and H. Yamauchi, *Chem. Mater.*, 2008, **20**, 6378–6381.
15 Y. Jia, H. Jiang, M. Valkeapää, H. Yamauchiä, M. Karppinen and E. I. Kauppinen, *J. Am. Chem. Soc.*, 2009, **131**, 4880–4883.
16 O. Parkkima, H. Yamauchi and M. Karppinen, *Chem. Mater.*, 2013, **25**, 599–604.
17 K. Sato, M. Yamaguchi, S. Fujita, K. Suzuki and T. Mori, *Catal. Commun.*, 2006, **7**, 132–135.
18 O. Parkkima, A. Silvestre-Albero, J. Silvestre-Albero and M. Karppinen, *Catal. Lett.*, 2014, **145**, 576–582.
19 Z. Zhang, D. Han, S. Wei and Y. Zhang, *J. Catal.*, 2010, **276**, 16–23.
20 A. Maignan, V. Caignaert, V. Pralong, D. Pelloquin and S. Hébert, *J. Solid State Chem.*, 2008, **181**, 1220–1226.
21 M. Boaro, F. Giordano, S. Recchia, V. D. Santo, M. Giona and A. Trovarelli, *Appl. Catal., B*, 2004, **52**, 225–237.
22 Z. Zhang, Y. Fan, Y. Xin, Q. Li, R. Li, J. A. Anderson and Z. Zhang, *Environ. Sci. Technol.*, 2015, **49**, 7989–7995.
23 T. Komiyama, T. Motohashi, Y. Masubuchi and S. Kikkawa, *Mater. Res. Bull.*, 2010, **45**, 1527–1532.
24 J. Oi-Uchisawa, A. Obuchi, S. Wang, T. Nanba and A. Ohi, *Appl. Catal., B*, 2003, **43**, 117–129.